Intermolecular Interactions between a Monomolecular Hydroxyl-Terminated Perfluoropolyether Film and the Sputtered SiNx Surface

R. J. Waltman,* B. K. Yen, R. L. White, and D. J. Pocker

Hitachi Global Storage Technologies, 5600 Cottle Road, San Jose, California 95193

G. W. Tyndall

IBM Almaden Research Center, 650 Harry Road, San Jose, California 95120

Received April 7, 2004. Revised Manuscript Received July 19, 2004

The intermolecular interactions at the interface between a monomolecular hydroxyl-terminated perfluoropolyether (PFPE) liquid and an amorphous silicon nitride (SiNx) film were investigated using contact angle goniometry, Fourier transform infrared spectroscopy, and X-ray photoelectron spectroscopy. The results demonstrate that the surface of the sputtered SiNx film is highly oxidized (SiO_2) and contain hydroxyl groups (SiOH) that are capable of attractive interactions with the hydroxyl end groups of the PFPE. The attractive interactions lead to a lowering of the polar surface energy with increasing PFPE coverage up to a monolayer. Ab initio quantum chemical computations on model dimers provide the energetic details associated with the PFPE/surface interactions. The primary source of the attractive, adhesive interactions in the PFPE/SiNx system stems from hydrogen bonding between the PFPE and SiNx hydroxyl groups. The binding energy is computed to be approximately −4 kcal/mol. Both the SiNx surface nitrogen and oxygen atoms in the Si_3N and Si−O−Si local geometries are weakly basic and hence incapable of providing strong adhesive interaction sites for the PFPE hydroxyl end groups. The results on the kinetics of the adhesive interactions between the hydroxyl-terminated PFPE and the SiNx surface demonstrate a nonclassical time-dependent rate coefficient, $k(t) \propto k_o t^{-h}$. With increasing temperature, the temporal dependence is observed to change from $h = 0.5$ (lower temperature) to $h = 1.0$ (higher temperature), which is interpreted as a two-dimensional melting transition from a solidlike to a liquidlike confined film. Under ambient conditions, adsorbed water competes with PFPE for surface bonding sites on the polar SiNx surface, leading to a significantly reduced level of adhesion for the hydroxyl-terminated PFPE.

Introduction

Over the past decade, the storage density of hard-disk drives has increased at a rate of approximately 60% per year. While these increases have been realized in part by the implementation of advanced magnetic alloys and sensor technologies, the reduction in the physical spacing between the read−write head and the rigid disk surface has played a major role. In today's hard disk drives, the mechanical clearance between the read−write head and the disk surface is less than ∼6 nm with the expectation that it will continue to decrease to as little as a few nanometers. At these small spacings, the topically applied lubricant film itself can mediate slider-disk interference.[1−3] Consequently, any attainable margin in clearance will continue to drive the design of the head−disk interface. The reduction in the thickness of the carbon overcoat continues to be one methodology by which the magnetic spacing is decreased. In the current practice, approximately 30−40 Å of an amorphous carbon film is typically deposited as the protective layer for the underlying magnetic film. To accommodate the anticipated storage density of 1 terabit/in,[2] the thickness of the carbon film is expected to be approximately 20 Å.

One concern with the continued use of sputtered carbon is its possible lack of robustness at the head−disk interface with decreasing film thickness. Below ∼30 Å sputtered carbon films appear to be less corrosion-resistant and the tribological robustness of the head−disk interface (HDI) is in question.[4,5] While substrate bias deposition[6] may prolong the use of sputtered carbon, ion beam carbon and/or cathodic arc carbon is expected to provide both increased hardness and uniformity at the reduced film thickness of ∼20−30 Å.[7−9] However, concerns over the possible delamination of these harder overcoat films at the carbon/magnetic layer

(1) Waltman, R. J.; Tyndall, G. W. *J. Magn. Soc. Jpn.* **2002**, *26*, 97.
(2) Khurshudov, A.; Waltman, R. J. *Trib. Lett.* **2001**, *11*, 143.
(3) Waltman, R. J.; Khurshudov, A. *Trib. Lett.* **2002**, *13*, 197.
(4) Mate, C. M.; Yen, B. K.; Miller, D. C.; Toney, M. F.; Scarpulla, M.; Frommer, J. *IEEE Trans. Magn.* **2000**, *36*, 110.
(5) Yen, B. K.; White, R. L.; Waltman, R. J.; Dai, Q.; Miller, D. C.; Kellock, A. J.; Marchon, B.; Kasai, P. H.; Toney, M. F.; York, B. R.; Deng, H.; Xiao, Q.-F.; Raman, V. *J. Vac. Soc. Technol. A* **2003**, *21*, 1895.
(6) White, R. L.; Bhatia, C. S.; Meeks, S. W.; Friedenberg, M. C.; Mate, C. M. *Tribology* **1996**, *6*, 33.

10.1021/cm040054y CCC: $27.50
Published on Web 11/04/2004

interface due to the higher residual stresses inherent in these films have also been cited.[9]

Investigations into alternative overcoat materials such as silicon nitride (SiNx) and nickel silicide have also been reported.[10−13] These materials exhibit superior corrosion resistance to amorphous carbon films due to their higher (electrical) resistivities and/or superior surface coverage.[5,14] However, the tribological properties of these materials are not well-understood and appear to vary significantly with the stoichiometry of the film (Si:N:O) and in particular to the extent of film oxidation.[12,13] Tribological robustness of the HDI has been linked to the mobility of the adsorbed lubricant thin film,[15] but presently there appears to be no fundamental understanding of the interactions between perfluoropolyether (PFPE) lubricants and the SiNx surface, which therefore provides the motivation for these studies.

We investigate the intermolecular interactions that develop between the hydroxyl-terminated perfluoropolyether (PFPE) lubricant Zdol and the SiNx surface. XPS and FTIR are utilized to qualitatively identify the surface functional groups present on the sputtered SiNx surface. The adhesive interactions that develop between the Zdol end groups and the SiNx surface sites are then determined by conducting experiments on the bonding and debonding kinetics of Zdol on SiNx and also by measurement of the changes in the surface energies of the disk surface as a function of Zdol film thickness. The decrease in the polar component of the surface energy with the lubricant film thickness is consistent with the interaction of the Zdol hydroxyl end groups with the polar sites on the SiNx surface. Hydrogen-bonding interactions are interpreted based upon ab initio quantum chemical modeling of lubricant end group interactions with possible SiNx surface sites. Collectively, these studies provide a fundamental understanding of the interactions between the Zdol lubricant and the SiNx surface.

Experimental Section

Materials. The substrates used in these studies were 65 mm diameter glass disks nominally of 8 Å RMS roughness and a peak roughness of approximately 20 Å. The substrate roughness was measured using a Dimension 5000 AFM with a standard AFM tip used in the tapping mode. The typical scan size was 10 μm × 10 μm with a scan rate of 0.5 Hz and 256 lines of resolution. Atop the glass substrates were sputter-deposited an underlayer of Cr, a cobalt-based magnetic layer, and nominally 25 Å of silicon nitride, SiNx. The sputtered SiNx overcoats were prepared by two methods for comparative purposes: (a) a radio frequency (13.56 MHz) rf-reactive sputtering and (b) dc-reactive sputtering, using Si targets (99.99% purity) in a N_2/Ar atmosphere.

The perfluoropolyether used in this work was obtained from Ausimont under the tradename Fomblin Zdol 4000. Zdol 4000 is a random copolymer of perfluoromethylene oxide and perfluoroethylene oxide monomer units capped by hydroxyl end groups. The Zdol 4000 was characterized by a number average molecular weight, M_n, of 3600, a perfluoromethylene oxide to perfluoroethylene oxide monomer unit ratio of 1.08, and >99% hydroxyl end groups as determined by NMR. Zdol was applied to the SiNx and/or CNx surfaces from solvent (hydrofluoroether solvent HFE-7100) using a standard dip-coating methodology, with a typical Zdol concentration of 0.5−1.0 g/L and a typical disk withdrawal rate of several mm/s.

$$HO-CH_2CF_2O-[CF_2O]_x-[CF_2CF_2O]_y-CF_2CH_2-OH$$

Zdol

Surface Energy Measurements. The surface energy for Zdol on SiNx and CNx were determined as a function of lubricant film thickness from contact angle measurements using a series of saturated alkanes ($\gamma_l^p = 0$ mJ/m^2) and water ($\gamma_l^d = 21.8$ mJ/m^2, and $\gamma_l^p = 51.0$ mJ/m^2) as the reference liquids. The methodology for these measurements is described elsewhere[16] so no extensive reiteration is necessary here. The contact angle, θ, made between a liquid and a solid surface is related to the free energy of the surface, γ_s, via Young's equation

$$\gamma_l \cos\theta = \gamma_s - \gamma_{sl} \tag{1}$$

where γ_l is the surface energy (tension) of the reference liquid and γ_{sl} is the solid−liquid interfacial energy. The dispersive component of the surface energy is determined from contact angle measurements using reference liquids capable of interacting with the surface via dispersive forces only (i.e., hexadecane). In this case, the solid−liquid interfacial energy, γ_{sl}, is given by[17]

$$\gamma_{sl}^d = \gamma_s^d + \gamma_l^d - 2\sqrt{\gamma_s^d \gamma_l^d} \tag{2}$$

The dispersive component of the surface energy is then obtained using the graphical technique of Fowkes. When the reference liquid is capable of interacting with the surface via both dispersive and polar forces, the interfacial energy can be approximated by[18,19]

$$\gamma_{sl} = \gamma_s + \gamma_l - 2\sqrt{\gamma_s^d \gamma_l^d} - 2\sqrt{\gamma_s^p \gamma_l^p} \tag{3}$$

which upon substitution into Young's equation readily provides an expression for the polar component of the surface energy. The total surface energy is then the sum of the dispersive and polar components.

XPS and FTIR Measurements. The sputtered SiNx films were characterized using XPS (X-ray photoelectron spectroscopy) and FTIR (Fourier transform infrared spectroscopy). The XPS measurements were made on a Physical Electronics Phi Quantum 2000 ESCA system employing monochromatic Al Kα irradiation. Measurements were conducted using grazing (5−15°) and near-perpendicular (75−90° detected cone axis) take-off angles. Since the goal of these studies was to investigate as closely as possible the SiNx surface as seen by Zdol as it

(7) Hyodo, H.; Yamamoto, T.; Toyoguchi, T. *IEEE Trans. Magn.* **2001**, *37*, 1789.
(8) Anoikin, F. V.; Yang, M. M.; Chao, J. L.; Russak, M. A. *J. Appl. Phys.* **1999**, *85*, 5606.
(9) Weiler, M.; Sattel, S.; Giessen, T.; Jung, K.; Ehrhardt, H.; Veerasamy, V. S.; Robertson, J. *Phys. Rev. B* **1996**, *53*, 1594.
(10) Yang, M. M.; Spaulding, D.; Chao, J. L.; Russak, M. A. *IEEE Trans. Magn.* **2000**, *36*, 2702.
(11) Wang, Z.; Yang, M. M.; Chao, J. L.; Russak, M. A. *IEEE Trans. Magn.* **1999**, *35*, 2361.
(12) Chen, G.-L.; Wu, J.; Weiss, J.*IEEE Trans. Magn.* **1999**, *35*, 2364.
(13) Wen, J.; Ying, X.; Wong, K.; Barth, G. *IEEE Trans. Magn.* **1999**, *35*, 2358.
(14) Tyndall, G. W.; Waltman, R. J.; Pacansky, J. *J. Appl. Phys.* **2001**, *90*, 6287.
(15) Karis, T. E.; Tyndall, G. W.; Waltman, R. J. *Trib. Trans.* **2001**, *44*, 249.
(16) Tyndall, G. W.; Waltman, R. J.; Pocker, D. J. *Langmuir* **1998**, *14*, 7527.
(17) Wu, S. *Polymer Interface and Adhesion;* Marcel Dekker: New York, 1982.
(18) Owens, D. K.; Wendt, R. D. *J. Appl. Polym. Sci.* **1969**, *13*, 741.
(19) Kaelbe, D. H. *J. Adhes.* **1970**, *2*, 66.

was applied, no sputter etching or other surface preparation of the SiNx film was done. System pressure during the measurements was in the 10^{-9} Torr range. Specular reflection FTIR (Nicolet Magna Model 560) was also used to characterize the SiNx surface and to quantify the film thickness of the applied perfluoropolyether Zdol. A standard specular reflection adapter (Harrick, New York) was used to maintain the proper angle of incidence to the sample. Infrared spectra on SiNx were obtained using 45 Å films deposited on metal substrates, with the incident infrared radiation at an angle equal to approximately 70°. The changes in the Zdol film thickness were quantified by relating the Zdol absorption band at 1282 cm^{-1}, due to the combination of C−F and C−O stretching vibrations, to film thickness as determined by XPS.[20] For these purposes, Zdol films of various thicknesses from approximately 7 to 18 Å were quantified via XPS to provide the thickness calibration. A standard (XPS) take-off angle (45 ± 15°) was used to determine the thickness of the Zdol films.

Throughout the following, we refer to the Zdol lubricant on the disk surface as being either "bonded" or "mobile." To clarify our definition of these terms, we briefly describe the methodology by which these quantities are determined. Following lubricant application, the initial lubricant thickness is measured via specular reflectance FTIR. The lubricated disks are then annealed for a specified period of time and the remaining lubricant film thickness is remeasured. The decrease in the lubricant thickness following annealing yields the evaporated amount. In the following, we report the evaporated fraction which is defined as the amount evaporated normalized to the initial thickness. After annealing, the disks are washed sequentially in hydrofluoroether (HFE-7100, 3M) and 2,3-dihydro-perfluoropentane (Vertrel-XF, DuPont) to remove any soluble lubricant, and the lubricant thickness is remeasured. The lubricant retained by the disk is defined to be the amount "bonded", while the portion removed by the solvent wash process is defined as the "mobile" lubricant. For bonded lubricant, our experiments do not distinguish between physi- and chemisorption. Again, the fraction bonded and the mobile fraction are obtained by normalizing to the initial lubricant thickness.

Computational Methodology. Ab initio calculations were performed using the Gaussian 98 computer code.[21] All geometries were fully optimized using the density functional theory (DFT) at either the 6-31G(d) or the 6-311++G(d,p) basis set.[22] For all computations, DFT calculations using Becke's 3-parameter functional[23] together with Perdew and Wang's gradient-corrected correlation functional[24] were employed. For all structures, differentiation of the energy gradients at the optimized geometries produced no imaginary frequencies. The molecular electronic properties are reported using the CHelpG population analyses.[25] Figures reproducing the computational results were made using the GaussView graphical user interface[26] and the CambridgeSoft graphical software.[27]

The strengths of the bonding interactions between the Zdol lubricant and the SiNx surface were quantified by dimer calculations on representative surface models. All dimer interaction energies were computed using electron-correlated wave functions at the 6-311++G(d,p) basis set. The 6-311++G(d,p) basis includes *d* functions for oxygen atoms, and *p* functions for hydrogen atoms, both of which are important for a quantitative description of hydrogen bonding. At the 6-311++G(d,p) basis set, the computed binding energies are expected to be close to the Hartree−Fock limit. The dimer binding energy is obtained as the difference between the total energies of the complex and the isolated reactants, i.e., $\Delta E = E_{AB} - (E_A + E_B)$, corrected for zero-point energy contributions.

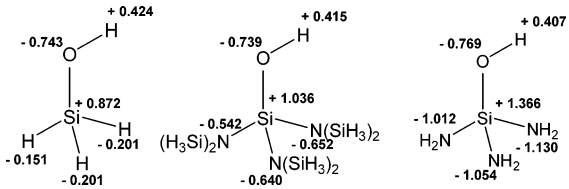

Figure 1. The computed ChelpG partial atomic charges on the B3PW91/6-311++G(d,p) optimized geometries of some R−SiOH surfaces with R equal to (left) H, (middle) $[H_3Si]_2N$, and (right) H_2N. No imaginary frequencies were computed for each of the optimized geometries. The Si−O−H bond angles (in degrees) are as follows: (left) 119.5; (middle) 119.9; and (right) 115.9. The R−Si−O−H torsion angles (in degrees) are as follows: (left) −178.9, −59.2, 61.5; (middle) −172.0, −54.3, 66.5; and (right) −170.0, −41.0, 74.3.

As stated above, model structures representative of each reactant at the Zdol/SiNx interface were employed to quantify the dimer interaction energetics. To keep the computations tractable at the 6-311++G(d,p) basis set, HCF_2CH_2OH was used to represent the Zdol hydroxyl end group and H_3SiOH was chosen to represent the silanol surface functionality. Other model structures were also considered for the R_3SiOH silanol surface, where R equaled either NH_2 or $N(SiH_3)_2$, to provide a more stoichiometrically representative surface model. However, these could not be employed for the following reasons. When R equaled $N(SiH_3)_2$, the local Si−N−Si optimized geometry had the expected planar geometry and this structure represented the smallest yet most accurate model for the idealized silanol surface based upon the Si_3N_4 stoichiometry. However, dimer computations at the 6-311++G(d,p) basis set were found to be prohibitively expensive during the course of these studies, leading us to consider a much smaller R group for the silanol surface model. When R equaled NH_2, the Si−N bonding could also be preserved and subsequent computations on the dimers were found to be computationally tractable. However, the optimized geometry centered at $Si-NH_2$ was pyramidal, leading to a relatively large, localized excess negative charge on the nitrogen atom of the $-NH_2$ group that served to decrease the acidity of the silanol hydrogen atom (Figure 1 right). Thus, H_3SiOH was selected as the best compromise between computational tractability and representative surface properties on the basis of the computed partial atomic charges for each of the silanol surface models. Figure 1 shows that the partial atomic charge computed on the silanol hydrogen atom in R_3SiOH is 0.424, 0.415, and 0.407 for R equal to H, $N(SiH_3)_2$, and NH_2, respectively. This is indicative that the acidity of the silanol OH functionality in R_3SiOH decreases in the following order: H > $N(SiH_3)_2$ > NH_2. A comparison of the computed negative charges on the silanol oxygen atom, −0.743, −0.739, and −0.769 for R equal to H, $N(SiH_3)_2$, and NH_2, respectively, indicates that the acidity of the silanol OH group is comparable for H and $N(SiH_3)_2$. This was verified in subsequent and limited dimer calculations showing comparable results for R equal to H and $N(SiH_3)_2$, to be compared in Figure 6 later. Thus, H_3SiOH was chosen to allow greater computational flexibility without sacrificing accuracy.

(20) Toney, M. F.; Mate, C. M.; Pocker, D. J. *IEEE Trans. Magn.* **1998**, *34*, 1774.
(21) Frisch, M. J.; Trucks, G. W.; Schlegel, H. B.; Scuseria, G. E.; Robb, M. A.; Cheeseman, J. R.; Zakrzewski, V. G.; Montgomery, J. A., Jr.; Stratmann, R. E.; Burant, J. C.; Dapprich, S.; Millam, J. M.; Daniels, A. D.; Kudin, K. N.; Strain, M. C.; Farkas, O.; Tomasi, J.; Barone, V.; Cossi, M.; Cammi, R.; Mennucci, B.; Pomelli, C.; Adamo, C.; Clifford, S.; Ochterski, J.; Petersson, G. A.; Ayala, P. Y.; Cui, Q.; Morokuma, K.; Malick, D. K.; Rabuck, A, D.; Raghavachari, K.; Foresman, J. B.; Cioslowski, J.; Ortiz, J. V.; Baboul, A. G.; Stefanov, B. B.; Liu, G.; Liashenko, A.; Piskorz, P.; Komaromi, I.; Gomperts, R.; Martin, R. L.; Fox, D. J.; Keith, T.; Al-Laham, M. A.; Peng, C. Y.; Nanayakkara, A.; Gonzalez, C.; Challacombe, M.; Gill, P. M. W.; Johnson, B.; Chen, W.; Wong, M. W.; Andres, J. L.; Gonzalez, C.; Head-Gordon, M.; Replogle, E. S.; Pople, J. A. *Gaussian 98*, Revision A.7; Gaussian, Inc.: Pittsburgh, PA, 1998.
(22) McLean, A. D.; Chandler, G. S. *J. Chem. Phys.* **1980**, *72*, 5639.
(23) Becke, A. D. *J. Chem. Phys.* **1996**, *104*, 1040.
(24) Perdew, J. P.; Burke, K.; Wang, Y. *Phys. Rev. B* **1996**, *54*, 16533.
(25) Breneman, C. M.; Wiberg, K. B. *J. Comput. Chem.* **1990**, *11*, 361.
(26) *GaussView 2.1*; Gaussian, Inc.: Pittsburgh, PA, 1998.
(27) *CambridgeSoft Chem 3D Ultra*, Version 4.0, Cambridge, MA, 2000.

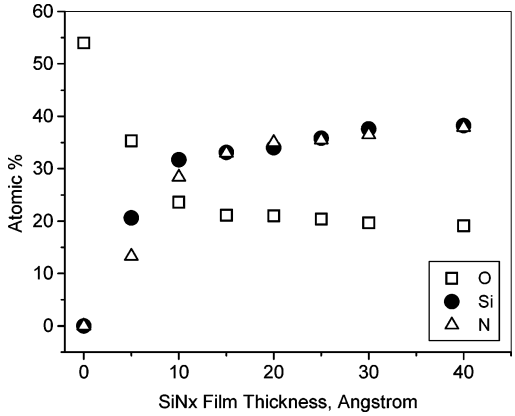

Figure 2. The atomic composition of SiNx films as a function of thickness for Si (●), N (△), and O (□). For the SiNx films of 0 and 5 Å, the contribution to the oxygen concentration due to the oxidation of the underlying magnetic film (Co) are 18.4 and 1.4 at. %, respectively.

Table 1. The H (at. %) Content in the Sputtered SiNx Film as a Function of Film Thickness

thickness, Å	Si (at. %)	N (at. %)	H (at. %)
504	43.7	54.1	2.2
552	43.0	55.1	1.9
575	44.3	54.0	1.6
693	42.6	56.1	1.2
951	44.8	54.4	0.8
1242	48.9	50.5	0.6

Results

Surface Composition of the Sputtered SiNx Surface. The atomic composition of SiNx as a function of film thickness was determined by XPS. As shown in Figure 2, the sputtered SiNx surface is highly oxidized, being comprised of approximately 20 at. % (atomic %) oxygen for film thicknesses between 15 and 40 Å. Within this film thickness range, the concentration of oxygen appears to decrease asymptotically from nominally 22 at. % at 15 Å to approximately 20 at. % at 40 Å. For film thicknesses below 10 Å, the oxygen concentration in excess of 20 at. % is attributed to the oxidation of both the SiNx and the underlying Co metallic film, i.e., the magnetic layer of the rigid disk.[5] Figure 2 also indicates that the Si:N ratio is approximately 1:1 for all film thicknesses between 15 and 40 Å. Thicker sputtered SiNx films (≳500 Å) produce SiNx films that are consistent with the bulk Si_3N_4 composition (Table 1).[5]

For the film thickness utilized in the Zdol−SiNx studies to be described below, nominally 25 Å SiNx, the stoichiometry of the sputtered SiNx film was determined to be $Si_{3.0}N_{3.0}O_{1.6}$ on the basis of the XPS results (Figure 2). This composition departs considerably from the expected Si_3N_4 bulk composition.[28−32] However, if the nitrogen and oxygen atoms are combined, the surface stoichiometry can be represented by $Si_{3.0}R_{4.6}$, where R is equal to the sum of the oxygen and nitrogen atomic percent. This is very close to an expected stoichiometry of $Si_{3.0}N_{3.0}O_{1.5}$ based upon the assumption that O is capable only of two covalent bonds (as Si−O−Si) while N is capable formally of three. The slight excess of oxygen in $Si_{3.0}N_{3.0}O_{1.6}$, coupled with the asymptotically decreasing oxygen content between 15 and 40 Å shown in Figure 2, suggests increased oxygen concentration near the SiNx surface.

Sputtered SiNx films were compared at grazing and near-perpendicular electron take-off angles to obtain additional information on the extent of film oxidation. Representative high-resolution Si 2p spectra obtained for a sputtered SiNx (40 Å) film are presented in Figure 3. The peak assignments for the composition of the SiNx film are made on the basis of reference Si 2p spectra for sputtered Si (50 Å) and for a Si wafer, also shown in Figure 3. The Si 2p spectrum for SiNx at the near-perpendicular take-off angle shows a broad peak at the binding energy of 102.1 eV. The corresponding grazing angle spectrum shows a broad peak centered at 102.5−103.2 eV that can be resolved into two major components centered at 102.0 and 103.2 eV. The 103.2 eV peak is readily assigned to SiO_2 as corroborated by the Si 2p spectra of sputtered Si and the Si wafer (Figure 3). Binding energies between 101.8 and 102.0 have previously been reported for authentic Si_3N_4.[31] Notably weak in the grazing angle spectrum for SiNx is the Si metal expected at the binding energy of 99.4 eV. This peak is evident as a readily recognizeable shoulder on the low binding energy side of the SiNx peak at a near-perpendicular take-off angle and is readily apparent in the grazing angle spectra for both sputtered Si and the Si wafer, Figure 3. Thus, the co-sputtering of Si with nitrogen precludes the formation of any significant Si−Si bonds. Insight into film composition as a function of film depth is provided by comparison of the relative intensity of the Si 2p peaks as a function of electron take-off angle. These data are summarized in Table 2. For SiNx, the ratio of the peak intensities at the grazing and near-perpendicular take-off angles indicates that film oxidation (to SiO_2) is significant near the air-exposed surface. Any excess Si (as Si metal) is nearest to the film/metal interface but represents only a minor constituent in sputtered SiNx (near-perpendicular spectrum). The layer thickness for each Si species was estimated from the Si 2p spectra, using electron mean free path values of 33.7 and 27.7 Å for SiO_2 and Si_3N_4, respectively.[33] The layers in the SiNx film are approximately 11 and 28 Å of SiO_2 and Si_3N_4, respectively, Table 2.

The surface oxidation of sputtered SiNx films was further investigated by measuring the H atomic percent as a function of the SiNx film thickness. For these purposes, FRS (Forward Recoil Spectrometry) was employed using a 2.3 MeV He^+ beam from a NEC 3UH Pelletron.[5] The data in Table 1 reveal that the H peak intensity increases toward the SiNx surface, which indicates that the measured H is due primarily to adsorbed contaminants such as water and/or hydro-

(28) Matsunaga, K.; Matsubara, H. *Mater. Res. Soc. Symp. Proc.* **1999**, *538*, 567.
(29) Ohdomari, I.; Yamakoshi, Y.; Kameyama, T.; Akatsu, H. *J. Non-Cryst. Solids* **1987**, *89*, 303.
(30) Misawa, M.; Fukunaga, T.; Nihara, K.; Hirai, T.; Suzuki, K. *J. Non-Crystal. Solids* **1979**, *34*, 313. Ayama, T.; Fukunaga, T.; Nihara, K.; Suzuki, K. *J. Non-Cryst. Solids* **1979**, *33*, 131.
(31) Ingo, G. M.; Zacchetti, N.; dellaSala, D.; Coluzza, C. *J. Vac. Sci. Technol.* **1989**, *A7*, 3048. Lee, G. U.; Chrisey, L. A.; O'Ferrall, C. E.; Pilloff, D. E.; Turner, N. H.; Colton, R. J. *Israel J. Chem.* **1966**, *36*, 81.
(32) Wang, P. S.; Malghan, S. G.; Hsu, S. M.; Wittberg, T. N. *J. Mater. Res.* **1993**, *8*, 3168.
(33) Tanuma, S.; Powell, C. J.; Penn, D. R. *Surf. Interface Anal.* **1991**, *17*, 927.

Table 2. XPS Data for Nominally 40 Å SiNx, 50 Å Si, and Si Wafer[a]

sample	peak assignment	B.E. (eV)	at. % grazing	at. % perpendicular	G/P ratio	thickness (Å)	composition
SiNx #1	Si (O_2)	102.5	13.7	6.9	2.0	11.8	SiO_2
	Si (N_x)	102.1	14.1	18.0	0.8	26.5	Si_3N_4
SiNx #2	Si (O_2)	103.2	12.7	5.8	2.2	11.3	SiO_2
	Si (N_x)	102.1	16.6	18.0	0.9	28.7	Si_3N_4
SiNx #3	Si (O_2)	102.5	13.9	6.5	2.1	11.3	SiO_2
	Si (N_x)	102.1	15.9	18.4	0.9	28.4	Si_3N_4
Si #1	Si (O_2)	103.4	16.0	9.5	1.7	16.2	SiO_2
	Si metal	99.4	14.5	34.4	0.4	54.0	Si
Si wafer	Si (O_2)	103.2	49.1	17.3	2.8	15.1	SiO_2
	Si metal	99.4	44.1	73.5	0.6	infinite	Si

[a] B.E. is the binding energy in eV for Si 2p. G/P ratio is the grazing to near-perpendicular ratio of the at. %. The Si wafer atomic composition refers only to the partitioning of the Si signals whereas all others (SiNx, Si) include all other detected elements.

carbon. The presence of both O and H therefore suggests that the oxidation of the sputtered SiNx films, in addition to the SiO_2, may be attributed to the truncation of unsatisfied bonds by oxygen species and/or water, possibly including dissociative attachment by water.[34–38] Conversely, the activation energy for the thermal oxidation of bulk Si_3N_4 is prohibitively high, >100 kcal/mol, at temperatures ≳1000 °C[39–41] and is not expected to contribute significantly here.

Further insight into the nature of the oxidized SiNx surface is provided by the specular reflectance infrared spectrum of a 45 Å SiNx film, Figure 4. The two major absorption bands at 1160 and 880 cm^{-1} are attributed to the stretching vibrations of SiO_2 and the in-plane Si−N.[42–44] The presence of both absorption bands in the infrared has been attributed to the existence of two locally separate phases, i.e., Si_3N_4 and SiO_2, within silicon nitride films.[45,46] Figure 4 also shows the presence of a smaller, sharp absorption band at 3750 cm^{-1}, which is due to the O−H stretching vibration of the silanol Si−OH group existing as the free, geminal, and vicinal functional groups.[47]

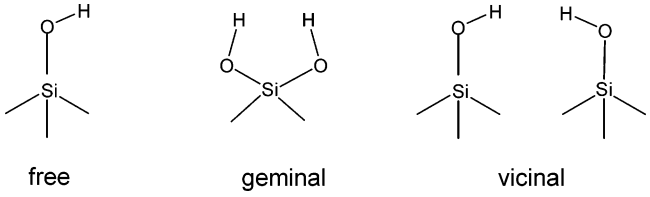

The same 3750 cm^{-1} absorption band in the infrared spectrum of sputtered Si films prepared identically as

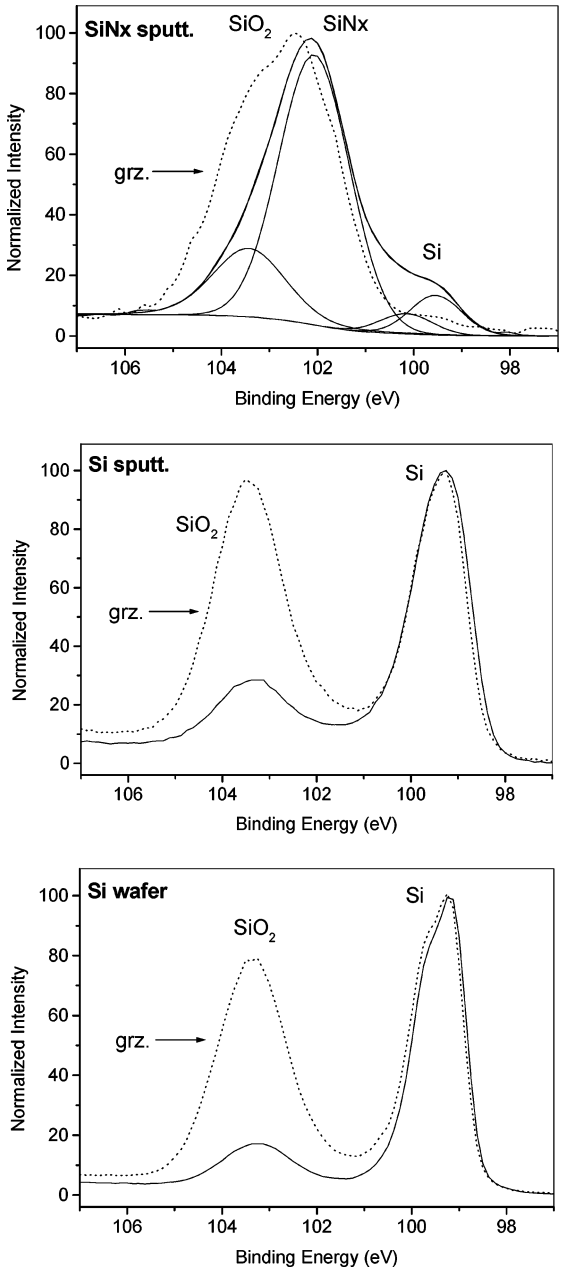

Figure 3. The Si 2p XPS spectra for (top) sputtered SiNx (40 Å), (middle) sputtered Si (50 Å), and (bottom) a polished Si wafer. The peak fits for the near-perpendicular SiNx spectrum are made on the basis of the SiO_2 and Si binding energies from authentic Si (middle, bottom figures). The near-perpendicular and grazing spectra are identified by the solid and dashed lines, respectively.

(34) Schalch, D.; Scharmann, A.; Wolfrat, R. *Thin Solid Films* **1987**, *155*, 301.
(35) Lewis, E. A.; Irene, E. A. *J. Vac. Sci. Technol.* **1986**, *A4*, 916.
(36) Franco, N.; Chrost, J.; Avila, J.; Asenio, M. C.; Muller, C.; Dudzik, E.; Patchett, A. J.; McGovern, I. T.; Giebel, T.; Lindsay, R.; Fritzsche, V.; Bradshaw, A. M.; Woodruff, D. P. *Appl. Surf. Sci.* **1998**, *123/124*, 219.
(37) Lacharme, J. P.; Sebenne, C.; Cherif, S. M.; Chikhi, M.; Safta, N.; Zaibi, M. A. *Appl. Surf. Sci.* **1993**, *65/66*, 598.
(38) Chabal, Y. J.; Christmas, S. B. *Phys. Rev. B* **1984**, *29*, 6974.
(39) Kuiper, A. E. T.; Willemsen, M. F. C.; Mulder, J. M. L.; Oude Elferink, J. B.; Habraken, F. H. P. M.; van der Weg, W. F. *J. Vac. Sci. Technol.* **1989**, *B7*, 455.
(40) Du, H.; Tressler, R. E.; Spear, K. E.; Pantano, C. G. *J. Electrochem. Soc.* **1989**, *136*, 1527.
(41) Enomoto, T.; Ando, R.; Morita, H.; Nakayama, H. *Jpn. J. Appl. Phys.* **1978**, *17*, 1049.
(42) Budhani, R. C.; Prakash, S.; Doerr, H. J.; Bunshah, R. F. *J. Vac. Sci. Technol.* **1987**, *A5*, 1644.
(43) Li, Y.-L.; Liang, Y.; Zheng, F.; Xiao, K.; Hu, Z.-Q. *J. Mater. Sci. Lett.* **1995**, *14*, 713.
(44) Liao, W.-S.; Lin, C.-H.; Lee, S.-C. *Appl. Phys. Lett.* **1994**, *65*, 2229.
(45) Franz, I.; Langheinrich, W. *Solid-State Electron.* **1971**, *14*, 499.

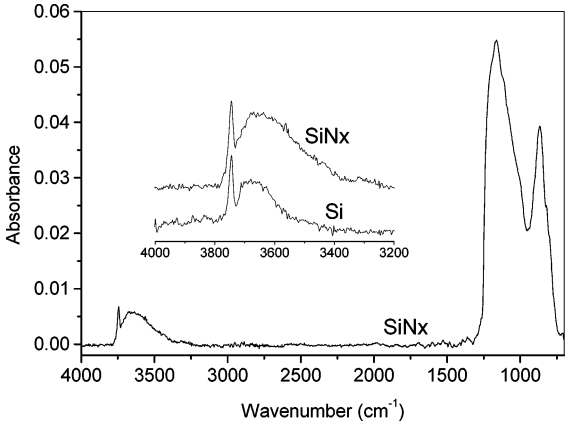

Figure 4. The reflectance infrared spectrum of the sputtered SiNx (45 Å) film. The inset figure highlights the O−H stretching region for the SiNx and the sputtered Si (50 Å) films.

the SiNx film but in the absence of a nitrogen flow is also shown in Figure 4. The presence of the identical OH band suggests that the surfaces are truncated in a similar manner by the ambient environment, producing silanol surface groups. The presence of SiOH surface groups has been observed by chemical extraction and electrochemical studies of silicon nitride powders.[31]

Surface Energies as a Function of Zdol Film Thickness on SiNx. As the perfluoropolyether Zdol is applied to the SiNx surface, a reduction in the surface free energy is observed. The dispersive and polar components of the surface energy for Zdol 4000 on SiNx as a function of lubricant thickness are shown in Figure 5. The dispersive surface energy per unit area, γ_s^d, represents the van der Waals dispersion forces acting between the perfluorinated ether backbone and the SiNx surface while the polar surface energy per unit area, γ_s^p, reflects the hydrogen bonding interactions between the lubricant hydroxyl end groups and the polar functional groups[48] on the SiNx surface. The total surface energy (per unit area) for the Zdol/SiNx interface is the sum of the two components, $\gamma_s = \gamma_s^d + \gamma_s^p$. The dispersive surface energy (γ^d) for the bare SiNx overcoat was determined to be 40 ± 5 mJ/m^2. Application of Zdol 4000 to the SiNx surface results in a decrease in the magnitude of γ^d that is film thickness dependent. Figure 5 shows that the dispersive surface energy, γ_s^d, decreases monotonically with increasing Zdol film thickness, asymptotically approaching the dispersive surface energy characteristic of bulk Zdol. Quantitatively, the dependence of $\Delta\gamma_s^d$ on the applied Zdol film thickness can be described using $\gamma^d(h) = \gamma_1^d + \Delta\gamma^d(h)$ where [49]

$$\Delta\gamma^d(h) = \frac{1}{12\pi}\frac{A^*}{(d_o + h)^2} \qquad (4)$$

where h is equal to the lubricant film thickness, d_o is a constant,[48] and A^* is the "effective" Hamaker constant.[50]

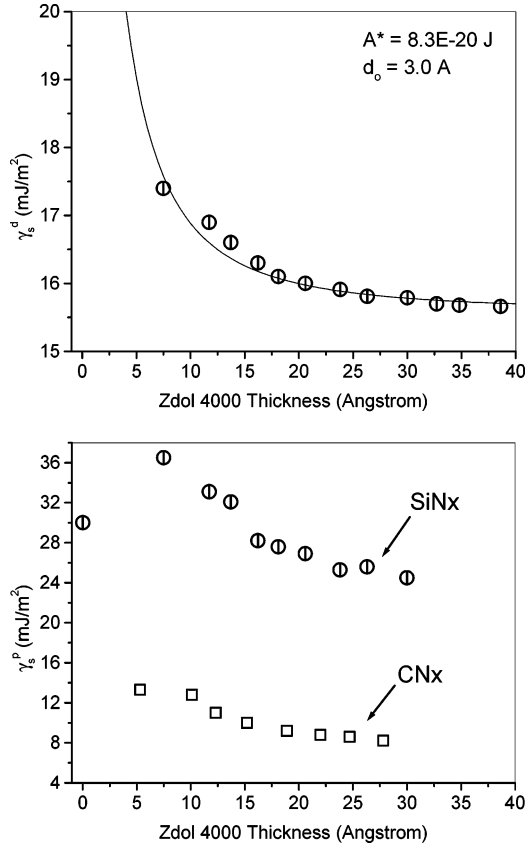

Figure 5. The (top) dispersive and (bottom) polar surface energies (mJ/m^2) for Zdol 4000 on SiNx as a function of Zdol film thickness. The polar surface energy for Zdol 4000 on CNx is also shown in the bottom figure to highlight the increased polarity of the SiNx surface. The surface energy measurements were made approximately 1−2 weeks after application of the lubricant film.

The effective Hamaker constant is defined as $A^* = A_{SL} - A_{LL}$, where A_{SL} and A_{LL} are the Hamaker constants describing the van der Waals interactions between the solid−liquid and the liquid−liquid interaction pairs, respectively. The solid line fit to the data shown in Figure 5 was obtained using eq 4 and $A^* = 8.3 \times 10^{-20}$ J, and $d_0 = 3.0$ Å. This indicates that the solid−liquid van der Waals interaction is repulsive for the Zdol/SiNx interface and is in qualitative agreement with the Zdol/CNx system discussed in detail previously.[16]

The d_o value used to fit the dispersive surface energy curve via eq 5, $d_o = 3.0$ Å, is indicative that the interaction between the Zdol nonpolar backbone (main chain) and the underlying surface is relatively weak and hence cannot provide any substantial adhesion. The interaction between the Zdol backbone and the SiNx surface was further investigated using quantum chemical ab initio calculations to compute the optimized distance between the lubricant backbone and the underlying surface. The optimized intermolecular distance was then compared to the d_o used to fit the dispersive surface energy data. In this study, the intermolecular interactions between a model lubricant backbone fragment, represented by CF_3OCF_3, and model silanol surface sites, represented by H_3SiOH and $[N(SiH_3)_2]_3$-SiOH, were computed. The results of the computations

(46) Chramova, L. V.; Smirnova, T. P.; Ayupov, B. M.; Belyi, V. I. *Thin Solid Films* **1981**, *78*, 303.
(47) Bermudez, V. M. *J. Phys. Chem.* **1971**, *75*, 3249.
(48) Waltman, R. J.; Tyndall, G. W.; Pacansky, J. *Langmuir* **1999**, *15*, 6470.
(49) Israelachvili, J. N. *Intermolecular and Surface Forces with Applications to Colloidal and Biological Systems*; Academic Press: London, 1985.
(50) deGennes, P.-G. *Rev. Mod. Phys*. **1985**, *13*, 837.

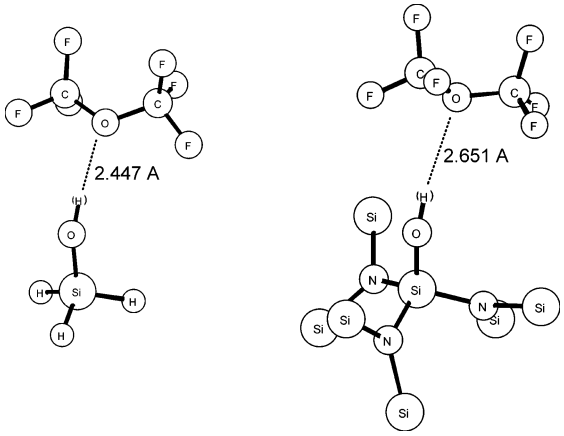

Figure 6. The B3PW91/6-311++G(d,p) optimized geometries for CF_3OCF_3 dimers with H_3SiOH and $[(SiH_3)_2N]_3SiOH$. No imaginary frequencies were computed for the dimers. For the $[(SiH_3)_2N]_3SiOH$ model surface, the three H atoms that are bonded to each Si atom in the $(SiH_3)_2N$ functional group are not displayed for ease of viewing the optimized dimer.

Table 3. B3PW91/6-311++G(d,p) Optimized Intermolecular Distances and Energies for Some Dimers (Figure 6)

dimer	distance, Å	ΔE, kcal/mol
$H_3SiOH + CF_3OCF_3$	2.447	−0.095
$[(SiH_3)_2N]_3SiOH + CF_3OCF_3$	2.651	−0.323

are presented in Figure 6 and summarized in Table 3. The distances of closest approach between CF_3OCF_3 and the H_3SiOH and $[N(SiH_3)_2]_3SiOH$ surfaces, respectively, are computed to be 2.45 and 2.65 Å, respectively. The optimized geometries in Figure 6 indicate that the silanol surface does not strongly interact with the perfluoroether backbone. Thus, the optimized geometries for the CF_3OCF_3/silanol dimers corroborate the negative Hamaker constant (A_{SL}) and the nonbonding d_o value determined from the fit to the dispersive surface energy data.

The polar component of the surface energy γ_s^p for the SiNx overcoats used in this work is nominally 30 mJ/m^2 and is considerably larger than the 10−20 mJ/m^2 typically measured on the CNx and CHx surfaces.[16] This is indicative that the SiNx surface is significantly more polar than the CNx and CHx surfaces. From the XPS and FTIR studies presented above, the polarity of the SiNx surface is tentatively attributed to the presence of silicon−oxygen and silicon−nitrogen functionalities. Application of the Zdol 4000 lubricant film to the SiNx overcoat strongly impacts the measured surface polarity, Figure 5. The addition of the lubricant to the SiNx surface in the thickness range of 0−30 Å results in a decrease in γ_s^p. The decrease in the polar surface energy with film thickness is reflective of an attractive polar interaction between the Zdol 4000 lubricant and the SiNx surface. Since the PFPE backbone is nonpolar, and hence incapable of a polar interaction, the observed surface energy decrease results directly from the interaction of the polar hydroxyl end groups of Zdol 4000 with the polar entities on the SiNx surface. This is attributed to the "bonding" interactions that develop between the Zdol hydroxyl end group and the polar functional groups on the SiNx surface. The properties

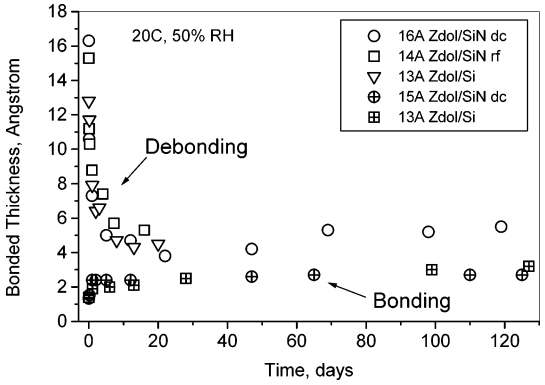

Figure 7. The changes in the bonded thickness of 13−16 Å Zdol 4000 on 25 Å SiNx and 50 Å Si as a function of time at 20 °C and 50 ± 5% relative humidity. The open symbols represent the debonding of Zdol as a function of time starting initially at 100% bonded thickness. The filled symbols represent the bonding of Zdol as a function of time starting initially at approximately 10% bonded thickness. The dc and rf in the figure legend refer to the dc- or rf-sputtering used to produce the SiNx film, as described in the Experimental Section.

of the bonding interactions are investigated via the kinetics described in the next section.

Ambient Bonding and Debonding Kinetics on SiNx. The results of the ambient bonding and debonding kinetic studies conducted with 12−14 Å of Zdol 4000 on SiNx at 20 °C and 50 ± 5% relative humidity (RH) are presented in Figure 7. When both the Zdol bonding and debonding kinetics are measured simultaneously, the asymptotic bonded fraction can be determined. The rate of lubricant debonding is followed as a function of time using initially 100% bonded lubricant on the SiNx surface. The disks with the 100% bonded Zdol 4000 are produced by annealing. The annealing temperature is selected to maximize the bonding rate but to minimize the evaporative loss which could otherwise change the molecular weight (MW) distribution of the fully bonded lubricant substantially.[48] Immediately after annealing, the disks are rinsed in solvent[51] (Vertrel-XF) to produce the 100% bonded disks which are subsequently monitored as a function of time. The disks are then measured for both the total and bonded lubricant film thicknesses. With increasing time the fraction of the lubricant that can be removed by the solvent increases, indicating that some of the bonded lubricant has converted to mobile lubricant. In Figure 7, we observe for Zdol 4000 on SiNx that both the bonded and debonded film thickness converge to an asymptotic film thickness of approximately 3−5 Å, corresponding to a bonded fraction of approximately 20−30% over the time range indicated. Figure 7 also shows that nearly identical kinetic data are obtained when the bonding and debonding experiments on Zdol 4000 are conducted on sputtered Si. These data suggest that the bonding between Zdol and the SiNx and Si surfaces result from similar intermolecular interactions and could derive from the silanol functional moiety. The nitrogen incorporated into sputtered SiNx therefore does not appear to promote Zdol bonding, which is opposite to the increased bonding

(51) Waltman, R. J.; Tyndall, G. W.; Wang, G. J.; Deng, H. *Trib. Lett.* **2004**, *16*, 215.

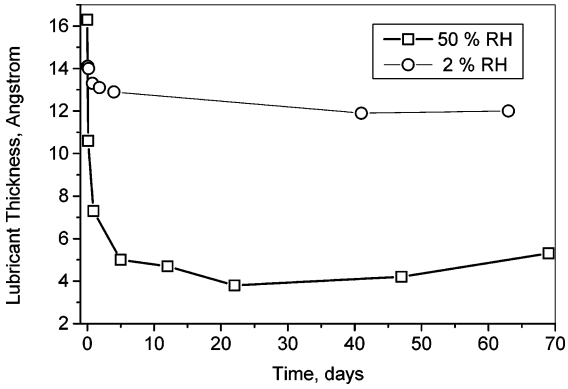

Figure 8. The debonding of 100% bonded Zdol 4000 on 25 Å SiNx at 20 °C and 2% and 50% relative humidity.

typically observed for Zdol on CNx compared to the CHx surface.[16,52]

The rapid debonding kinetics observed for Zdol on SiNx, coupled with the limited bonding of Zdol on SiNx, are indicative that competitive reactions are taking place on the SiNx surface that do not favor Zdol bonding under ambient conditions. This is to be contrasted to the adhesion of Zdol on amorphous hydrogenated and/or nitrogenated carbon surfaces where a bonded fraction of about 50% is readily attained under similar conditions.[53] We assume that the bonded lubricant on SiNx is displaced by the water that is adsorbed on the disk surface due to the relatively high polarity of the oxidized SiNx surface. This conclusion is based upon additional debonding kinetics studies conducted on Zdol 4000 on SiNx as a function of relative humidity. Figure 8 shows that the debonding of Zdol on SiNx is significantly reduced when the bonded lubricant is placed in a low humidity environment (2% RH). After 60 days under these conditions, only ~10% of the bonded lubricant has been converted to mobile lubricant.

Bonding Kinetics on SiNx at Elevated Temperatures. The results of the bonding kinetic studies conducted with 10 Å of Zdol 4000 on SiNx between 64 and 150 °C and ≤4% relative humidity (RH) are presented in Figure 9. Upon application of Zdol 4000 to the SiNx surface, a small fraction (~5−10%) of the lubricant bonds at room temperature within the time required to allow for solvent evaporation and to conduct the initial thickness measurements, Figure 9 (middle). This quantity of bonded lubricant is referred to as the initial bonded fraction, while the quantity of lubricant that is not bonded to the disk surface is referred to as the initial mobile fraction, Figure 9 (top). With increasing anneal time, the fraction of mobile Zdol 4000 present on the SiNx surface decreases and is quantitatively accounted for by both the increase in the bonding of the lubricant to the SiNx surface and the increase in the evaporation of the lubricant from the SiNx surface, Figure 9 (bottom). At the anneal temperature of 64 °C, the loss of mobile lubricant due to evaporation is a minor reaction channel accounting for less than ≲5% of the total lubricant thickness loss. However, as a function of increasing temperature, the loss of mobile lubricant due to evaporation increases where, at the maximum

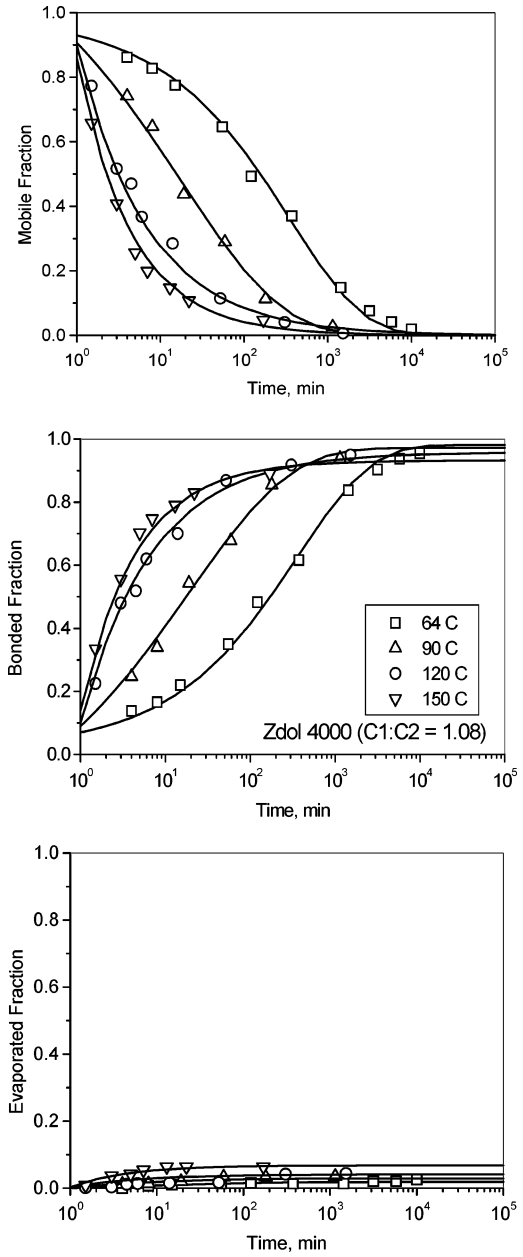

Figure 9. The changes in the mobile (top), bonded (middle), and evaporated (bottom) fractions of Zdol 4000 on 25 Å SiNx as a function of time and temperature from 64 to 150 °C. All initial lubricant film thicknesses were 10.5 ± 0.5 Å. The solid lines are the results of calculations derived from the theoretical rate laws in eqs 5−7.

temperature of 150 °C, we observe a ~10% loss of mobile lubricant.

Figure 9 also indicates that the bonding rate of Zdol 4000 on SiNx increases significantly with increasing temperature. For example, at 64 °C a 50% bonded fraction can be attained in ~200 min while at the highest temperature of 150 °C a 50% bonded fraction is achieved in only 2−3 min. This rapid bonding on SiNx also limits the evaporative loss of Zdol from the SiNx surface at the higher temperatures.

The bonding rate for Zdol 4000 on SiNx as shown in Figure 9 does not follow classical kinetics but instead is time-dependent with a rate coefficient that decreases with time. The theoretical fits accompanying the bonding data can be developed assuming a rate coefficient

(52) Waltman, R. J.; Tyndall, G. W.; Pacansky, J.; Berry, R. J. *Trib. Lett.* **1999**, *7*, 91.
(53) Waltman, R. J. *Chem. Mater.* **2004**, *16*, 62.

Table 4. Kinetic Data Obtained from the Fits to the Bonding and Evaporation of 10.5 Å Zdol 4000 on 25 Å SiNx

temperature, °C	k_B	k_C	h
64	0.026	0.004	0.50
90	0.120	0.009	0.63
120	0.490	0.022	1.00
150	0.610	0.050	1.00

that is time-dependent, i.e., $k(t) \propto k_o t^{-h}$, where $k(t)$ is the instantaneous rate coefficient at time t, k_o is the time-independent initial rate constant, and h is the coefficient describing the power function in time. Thus, the differential rate equations describing the depletion of mobile lubricant, A, the formation of bonded lubricant, B, and the evaporation of lubricant, C, may be written as[52]

$$\frac{dB}{dt} = k(t)A = k_B t^{-h} A \tag{5}$$

$$\frac{dC}{dt} = k(t)A = k_C t^{-1} A \tag{6}$$

$$-\frac{dA}{dt} = \frac{dB}{dt} + \frac{dC}{dt} \tag{7}$$

where k_B and k_C are the initial rate constants for bonding and evaporation, respectively. The results of the calculations based on this model are shown in Figure 9 as the solid lines. The mobile, bonded, and evaporated fractions in the y-axes in Figure 9 are presented as dimensionless film thicknesses normalized to the initial film thicknesses for each measured quantity. In all cases, the functional form of the time dependence in the evaporation channel follows an inverse time dependence as described previously.[54] For the bonding of Zdol on SiNx at 64 °C, the rate coefficient follows a $k(t) \propto k_B t^{-0.5}$ temporal dependence. The time dependence is a result of the formation of a nonrandom spatial distribution of the reactants, i.e., a segregation of reactant pairs or a "depletion zone," which arises from the fact that diffusion is not an effective self-stirring mechanism.[55] The diffusion-limited bonding results from the ability of the lubricant molecules to spatially deliver the polar functional end groups to the active sites on the SiNx surface.

From the theoretical curves accompanying the bonding kinetics of Zdol 4000 on SiNx, Figure 9, the power exponent h is observed to increase with temperature from 0.50 at 64 °C to 0.63 at 90 °C and to 1.00 for temperatures ≥120 °C (Table 4). A similar change in h was reported previously for the bonding kinetics of Zdol 4000 on CHx (amorphous hydrogenated carbon) as a function of main chain flexibility.[52] In those studies, the increase in h from 0.50 to 1.00 was associated with an increase in the configurational entropy of the adsorbed Zdol film that represented a "melting" of the confined Zdol liquid from a solidlike to a liquidlike state. This was subsequently corroborated by shear-modulated scanning force microscopy (SFM), which was used to probe the viscoelastic properties of molecularly thin Zdol films confined by the CHx surface.[56] By analogy, the kinetic data presented in Figure 9 suggests that the flexible Zdol used in these studies (C1:C2 = 1.08) undergoes a similar melting transition on the SiNx surface from a solidlike to a liquidlike film with increasing temperature.

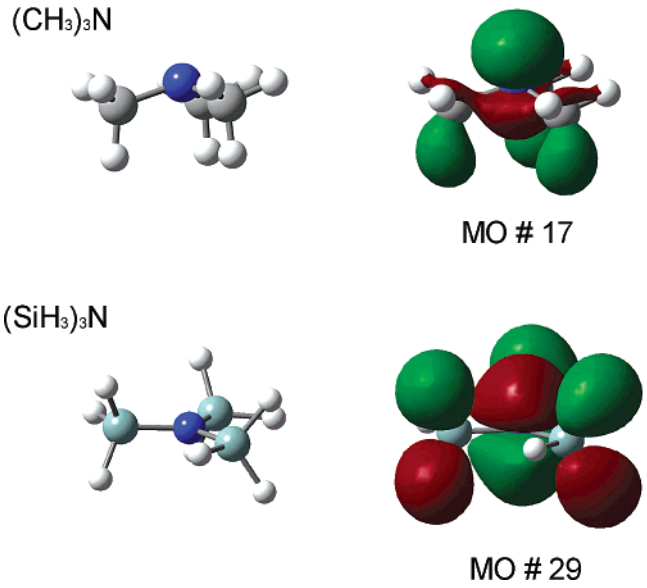

Figure 10. Molecular orbital plots at the B3PW91/6-31G(d) basis set.

Discussion

As discussed above, the bonding of the perfluoropolyether Zdol to the SiNx surface is energetically driven by the decrease in the free energy that results from the interaction of the Zdol polar −OH end groups with the polar sites on the SiNx surface. XPS data revealed that the SiNx surface was oxygen-rich with an indicated stoichiometry of $Si_{3.0}N_{3.0}O_{1.6}$. XPS and FTIR also detected the presence of SiO_2 and the terminal Si−OH group. Therefore, the most likely functional groups on SiNx to which Zdol can "bond" are Si_3N, SiO_2, and SiOH. We first assess the polarity of these functional groups and their ability to interact with the Zdol hydroxyl end group by computing their electronic structure via ab initio quantum chemical modeling. The focal point of these studies is to determine the relative acid/base properties of the surface functional groups compared to the Zdol hydroxyl end group and a surface contaminant like water. The results of the calculations may then be applied to the observed bonding and debonding of Zdol on SiNx as discussed in Figures 7 and 8. We begin the theoretical analyses by presenting the molecular orbital (MO) for the optimized geometry of Si_3N as an illustrative example. The MO contour for Si_3N in Figure 10 shows that the nitrogen lone pair of electrons occupies the $2p_z$ orbital, which interacts with the empty Si 3d orbitals forming a d(π)-p(π) bond. Consequently, the local Si_3N geometry is planar and the nitrogen lone pair of electrons are not available for hydrogen bonding. This is to be contrasted to the carbon analogue C_3N (trimethylamine), Figure 10, where the carbon atoms have

(54) Tyndall, G. W.; Waltman, R. J. *J. Phys. Chem. B* **2000**, *104*, 7085.

(55) Kopelman, R. *Science* **1988**, *241*, 1620.

(56) Waltman, R. J.; Buenviaje, C. K.; Frommer, J.; Overney, R. M.; Tyndall, G. W. Manuscript to be submitted, 2004.

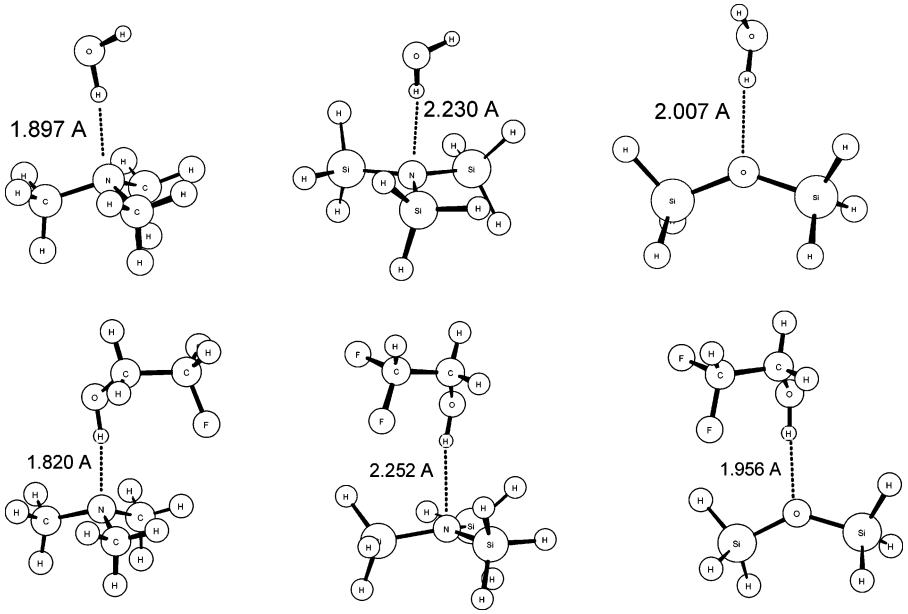

Figure 11. The B3PW91/6-311++G(d,p) optimized dimers of SiNx surface models with (top) water and (bottom) HCF_2CH_2OH (Zdol model). The optimized interatomic distances are given in angstroms. No imaginary frequencies were computed at the optimized dimer geometries.

no low energy d orbitals available for bonding with the central nitrogen atom; hence the σ bonding determines its pyramidal geometry. In this configuration, the nitrogen lone pair of electrons are available for hydrogen bonding. Thus, Si_3N is computed to be a weak base compared to the analogous C_3N structure. Similar analyses of the molecular orbitals for the Si−O−Si bridge in SiO_2, hereafter referred to as Si_2O, also show that the oxygen lone pairs of electrons interact with the empty Si 3d orbitals forming the d(π)-p(π) bond similar to that already discussed for Si_3N. Therefore, Si_2O is computed to be a much weaker base than the analogous carbon C_2O structure. The results of the computations are indicative that the nitrogen atom in Si_3N and the oxygen atom in Si_2O are not strongly basic surface sites.

The ability of the nitrogen atom in Si_3N and the oxygen atom in Si_2O to participate in hydrogen bonding reactions is next discussed. These important details are further investigated by computing the dimer interactions of these surface models with both water and HCF_2CH_2OH (the Zdol model). The optimized geometries of the dimers of Si_3N, Si_2O, and C_3N with water are shown in Figure 11. For the Si_3N-H_2O dimer, the N- - -H distance is computed to be 2.230 Å, which far exceeds a conventional hydrogen bond distance. Similarly for the Si_2O-H_2O dimer, the O- - -H distance is 2.007 Å and thus, by analogy, hydrogen bonding (at least of water) to the Si−O−Si bridge is not expected to be important. Conversely, the N- - -H distance in the hydrogen-bonded C_3N-H_2O dimer is the expected 1.897 Å. This is consistent with the observation of the excellent solubility of trimethylamine in water. The binding energies for the Si_3N-H_2O, Si_2O-H_2O, and C_3N-H_2O dimers are +0.39, −0.47, and −4.73 kcal/mol, respectively, as summarized in Table 5. These data are indicative that no significant hydrogen bonding is expected between Si_3N and H_2O and Si_2O and H_2O.

The optimized geometries for the dimers of HCF_2CH_2OH ("Zdol") with Si_3N, Si_2O, and C_3N are also presented in Figure 11. From the previous discussions on the surface-water dimer calculations, the Zdol−Si_3N and Zdol−Si_2O interactions are analogously computed to be considerably weaker than otherwise expected of normal hydrogen bonds despite the increased acidity of the Zdol hydroxyl end group. For Zdol−Si_3N the nonbonding close contact is 2.252 Å with a computed binding energy of +0.255 kcal/mol, Table 5. Clearly, we expect no hydrogen bonding to occur between the Zdol end group and Si_3N. As reference, the Zdol−C_3N hydrogen bonding interaction provides the expected H-bond distance of 1.820 Å with a computed binding energy of −6.508 kcal/mol. For the Zdol−Si_2O dimer, the optimized nonbonding close contact is 1.956 Å with a corresponding binding energy of −1.205 kcal/mol, Table 5. Due to the increased acidity of the Zdol −OH end group, the nonbonding close contact is considerably shorter than that of the H_2O-Si_2O dimer (2.007 Å) but still exceeds the typical hydrogen bond length of ∼1.8 Å. The computed binding energy of −1.205 kcal/mol is indicative of a weak binding interaction, between Zdol and Si−O−Si, Table 5. The results of these studies indicate that both the Si_3N and Si−O−Si are not strongly basic, leaving the SiOH functional group, to be discussed below, as the primary surface-active site that is available for hydrogen bonding.

Table 5. B3PW91/6-311++G(d,p) Optimized Intermolecular Distances and Energies for Some Dimers (Figure 11)

dimer	distance, Å	ΔE, kcal/mol
$(CH_3)_3N + H_2O$ (top, left)	1.897	−4.733
$(SiH_3)_3N + H_2O$ (top, middle)	2.230	+0.393
$(SiH_3)_2O + H_2O$ (top, right)	2.007	−0.473
$(CH_3)_3N + HCF_2CH_2OH$ (bottom, left)	1.820	−6.508
$(SiH_3)_3N + HCF_2CH_2OH$ (bottom, middle)	2.252	+0.255
$(SiH_3)_2O + HCF_2CH_2OH$ (bottom, right)	1.956	−1.205

A comparison of the optimized distances and the binding energies between the water and the Zdol dimers with the Si_3N, Si_2O, and C_3N surfaces indicate a

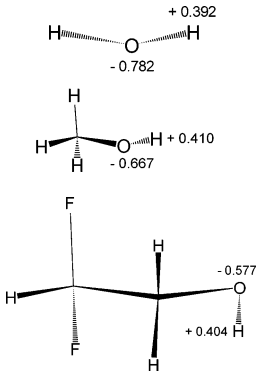

Figure 12. The partial atomic charges (ChelpG) for (top) water, (middle) methanol, and (bottom) HCF_2CH_2OH (Zdol model) at the B3PW91/6-311++G(d,p) optimized geometries.

stronger surface interaction for Zdol compared to water (in the absence of solvation effects). This is attributed to the fact that, in the gas phase, the acidity of the Zdol hydroxyl end group is greater than that of water, Figure 12, which accounts for the increased adhesion (hydrogen bonding) computed on the relatively weaker basic sites, Figure 11. Thus, the relative acidity decreases in the order $CHF_2CH_2OH > CH_3OH > H_2O$ as the negative charge on the oxygen atom increases. The electron-withdrawing CF_2 group adjacent to the CH_2OH end group in Zdol stabilizes the anion, thereby increasing the acidity of the alcohol end group relative to water.

Since hydrogen bonding between Zdol and the Si_3N and Si_2O surfaces is computed to be relatively unimportant, the expectation based on the experimental and theoretical studies presented thus far is that the surface site responsible for the adhesion of Zdol to SiNx is primarily silanol. To characterize these intermolecular interactions further, the hydrogen bonding interactions between HCF_2CH_2OH and H_3SiOH were also quantified by ab initio calculations. Figure 13 (bottom) shows the optimized geometries for two possible dimer interactions between the Zdol hydroxyl end groups and the acidic and basic silanol surfaces. The H-bonding distances are computed to be 1.858 and 1.866 Å, respectively, with the corresponding H-bond energies of $\Delta E = -4.120$ and -3.867 kcal/mol, respectively. The results of the calculations slightly favor H_3SiOH as an acidic site, by a modest $\Delta E = -0.253$ kcal/mol. However, the fact that at least one unshared lone pair of electrons remains on the oxygen atom of the SiOH functional moiety is consistent with the observation that silanol retains considerable basic character despite its strong acidity.[57]

Similar results are reported on dimer calculations between water and silanol, Figure 13 (top). A stronger H-bond is formed between acidic H_3SiOH and water. The H-bonding distances are computed to be 1.856 Å and a significantly longer 1.928 Å for water dimers with acidic and basic silanol, respectively, with the corresponding H-bond energies of $\Delta E = -4.418$ and -2.937 kcal/mol, respectively.

The results of the studies discussed above have demonstrated the ability of the hydroxyl-terminated

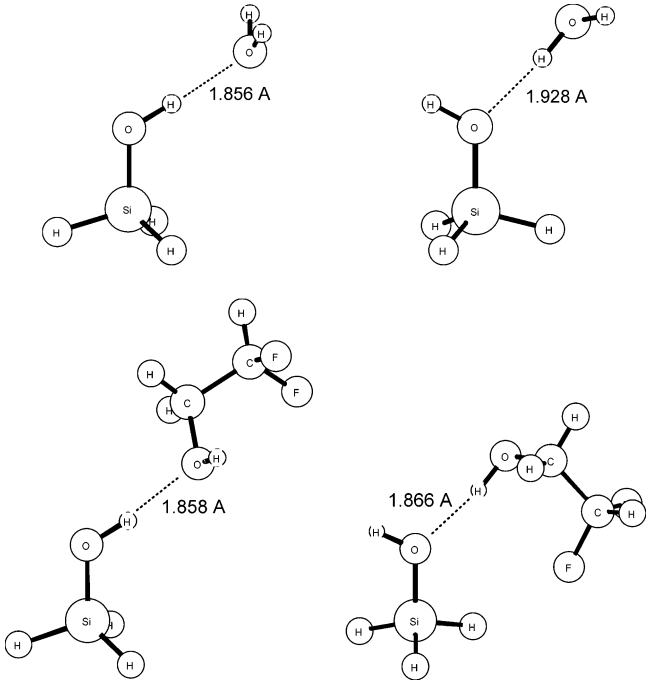

Figure 13. The B3PW91/6-311++G(d,p) optimized dimers of SiNx silanol surface models with (top) water and (bottom) HCF_2CH_2OH (Zdol model). The optimized interatomic distances are given in angstroms. No imaginary frequencies were computed at the optimized dimer geometries.

Table 6. B3PW91/6-311++G(d,p) Optimized Intermolecular Distances and Energies for Some Dimers (Figure 13)

dimer	hydrogen bond, Å	ΔE, kcal/mol
$H_3SiOH + HCF_2CH_2OH$	1.858	−4.120
$H_3SiOH + HCF_2CH_2OH$	1.866	−3.867
$H_3SiOH + H_2O$	1.856	−4.418
$H_3SiOH + H_2O$	1.928	−2.937

Zdol perfluoropolyether lubricant to bond to SiNx under elevated temperatures. However, we have also observed that bonded Zdol on the SiNx surface is readily displaced by water under ambient conditions. The previously discussed theoretical data indicated that both water and Zdol could form hydrogen bonds to the SiOH surface, Figure 13 and Table 6. For the acidic H_3SiOH silanol group, the computed H-bond energies for the H_3SiOH/H_2O and H_3SiOH/Zdol dimers were similar, −4.42 and −4.12 kcal/mol, respectively. For basic H_3SiOH, the computed H-bond energies for the H_3SiOH/H_2O and H_3SiOH/Zdol dimers were −2.94 and −3.87 kcal/mol, respectively. The results of the computations suggest that a water molecule can compete energetically with the Zdol hydroxyl end group to form a H-bond of similar strength, at least to the acidic H_3SiOH surface site. The energetic driving force for the displacement of the Zdol H-bond with a water H-bond on the SiNx surface may be attributed to the fact that an alcohol end group (Zdol) can have a maximum of 3 H-bonds while water can have a maximum of 4 H-bonds per molecule.[58] The ability of water to thus self-associate[59] and possibly form longer-range order on the polar SiNx surface compared to Zdol could allow for the facile displacement of the Zdol/SiNx hydrogen bond by water.

(57) The acid−base character of the underlying surface has been demonstrated to impact the adsorbed film structure, mobility, and the bonding kinetics of Zdol.[16] See also: Waltman, R. J.; Zhang, H.; Khurshudov, A.; Pocker, D. J.; Karplus, M.; York, B.; Xiao, Q.-F.; Zadoori, H.; Thiele, J.-U.; Tyndall, G. W. *Trib. Lett.* **2002**, *12*, 51.

Conclusions

The goal of these studies was to provide insight into the intermolecular interactions that occur between the hydroxyl-terminated perfluoropolyether Zdol and the sputtered, amorphous SiNx surface. It was found that the sputtered SiNx film contained appreciable surface oxidation as SiO_2 and SiOH, leading to a significantly higher polarity of the SiNx surface (30 ± 5 mJ/m^2) compared to sputtered amorphous hydrogenated- and nitrogenated-carbon (12 ± 4 mJ/m^2). The polar component of the surface energy could be reduced with increasing Zdol coverage due to the interaction of the Zdol hydroxyl end groups and the polar surface sites on SiNx. Based upon the results of ab initio computational modeling, it was concluded that the oxidized surface sites on SiNx provided the primary surface adhesion sites for Zdol since the nitrogen atoms in the Si_3N local geometry were weakly basic and hence incapable of interacting strongly with the Zdol hydroxyl end groups. It was also demonstrated that while the Zdol hydroxyl end group could adhere (or bond) to the SiNx surface, it could also be readily displaced by water present in the ambient environment. Thus, bonded Zdol underwent rapid debonding to reach an asymptotic bonded level of only 20−30%. It is anticipated that the mobile lubricant system as provided by the Zdol/SiNx interface could impact the tribological reliability of the hard-disk drive in a variety of ways that is contingent upon the desired goal of the head−disk interface. For example, it can be anticipated that the Zdol/SiNx system could perform well in tests that are designed to favor mobile lubricant, such as contact−start−stop, or more poorly in tests that are designed to favor bonded lubricant, such as higher RPM spin-off.

CM040054Y

(58) Knozinger, H. *The Hydrogen Bond III. Dynamics, Thermodynamics, and Special Systems*; North-Holland Publishing Co.: Amsterdam, 1976.

(59) Hankins, D.; Moskowitz, J. W.; Stillinger, F. H. *J. Chem. Phys*. **1970**, *53*, 4544.